Turbidimetric method for the determination of particle sizes in polypropylene/clay-composites during extrusion

Wolfgang Becker[a+], Viktor Guschin[a], Irma Mikonsaari[a], Ulrich Teipel[b], Sabine Kölle[a], Patrick Weiss[a]

[a] Fraunhofer Institute for Chemical Technology (Pfinztal, Germany)

[b] Technische Hochschule Nürnberg (Nürnberg, Germany)

+Corresponding author: Tel. ++49 (0)721 4640154; Email: Wolfgang.Becker@ict.fraunhofer.de; Fax: ++49 (0)721 4640111

Keywords: turbidimetry, particle, clay-composite, particle distribution, process monitoring

1. Abstract

Nanocomposites with polypropylene as matrix material and nanoclay as filler were produced in a double twin screw extruder. The extrusion was monitored with a spectrometer in the visible and near infrared spectral region with a diode array spectrometer. Two probes were installed at the end at the extruder die and the transmission spectra were measured during the extrusion. After measuring the transmission spectra and converting into turbidity units the particle distribution density was calculated via numerical linear equation system. The distribution density function show either a bimodal or mono modal shape in dependence of the processing parameters like screw speed, dosage and concentration of the nanoclays. The method was verified with SEM measurements which yield comparable results. The method is suitable for industrial in-line processing monitoring of particle radii and dispersion process, respectively.

2. Introduction

Effectivity and targeted production is one of the outmost characteristics of industrial production. Polymer processing is one of the biggest industrial sectors. Sophisticated process and material control is one of the most important competitive advantages in machine construction and its importance will grow in the future. Composites with added nanoparticles so called nanocomposites (NC) are gaining increasing attentiveness. The use of functional nanoparticles in polymers is one of the most promising but also one of the most challenging uses of this new material class. Low quantities of nanoparticles in these polymer nanocomposites can improve barrier properties to reduce gas diffusion, fire resistance, electrical conductivity, antistatic enhancement, optical properties and/or mechanical properties [1–3]. A main hurdle in commercialization is the uncertainty regarding the quality of the compounded material, which still shows a significant variation. In contrast to conventional fillers, the properties achieved with nanoparticles depend much more on a precisely controlled

dispersion, de-agglomeration and distribution of the filler in the polymer composite. Especially in case of the clay layer material which are adhered to each other forming compact entities these layers must be separated to unveil single the clay plates with thicknesses in the nanometer range. Unfortunately today's state of the art in characterizing these dispersion properties involves the use of time- and cost-intensive offline methods. This results in comparably high technical and economic risks and waste streams for the mainly SME-based nanocomposite manufacturers, as the most important properties of the composites can only be determined long after the production. The substantial lack in profound process understanding furthermore results in trial and error optimization and the fixed dispersion characteristics of conventional compounding technology – where a fixed machine setup is configured and then used throughout the [4] production - does not allow the necessary adaptation of dispersion during one production lot. Consequently the dispersion is more or less a function of the material input quality, with all the negative effects this has on the composite properties. Hence this study focusses on the development of an in-line applicable spectroscopic method for the determination of dispersion quality and particle size in the nanocomposite during processing in a compounding line. Spectroscopy in the visible and near infrared spectral range can be used as a rugged and fast in-line measurement system surveying the process and characterizing specific material and process properties [5–9]. The information of the scattered light caused by the imbedded particles was used to determine particle radius and their size distribution with turbidimetric method and evaluation [4, 10–12]. The method is not intended to replace a precise laboratory particle measurement method but to offer a rugged and stable processing in-line method for process and product control with particles involved.

3. Materials and methods

As an exemplary material system nanoclays, consisting of montmorillonite ($(Na,Ca)_{0,33(}Al,Mg)_2Si_4O_{10}(OH)_2nH_2O$) modified with a quaternary ammonium salt and with a two dimensional platelet shape were used. The nanoclay material was supplied by the company Southern Clay Products. Table 1 lists the properties of the nanoclay material in

detail. Figure 1 shows SEM pictures of pure Nanoclay material. Nanoclays were one of the first nanoparticles tested as filler for polymeric matrices and are now introduced to the compounding market in industrial scale. The increasing importance of NC with nanoclays is nowadays also recognized in a growing number of applications.

Table 1: Properties and material parameter of the nanoclay material

Tradename	Cloisite® 15A, Southern Clay Products (today BYK-Chemie)
Structural formula	$(Na,Ca)_{0,33(}Al,Mg)_2Si_4O_{10}(OH)_2nH_2O)$
Organic modifier	Dimethyl, dehydrogenated tallow, quaternary ammonium
Color	Off white
Density	1,66 g/cm³
Particle size	10 % < 2 µm
classes	50 % < 6 µm
	90 % < 13 µm

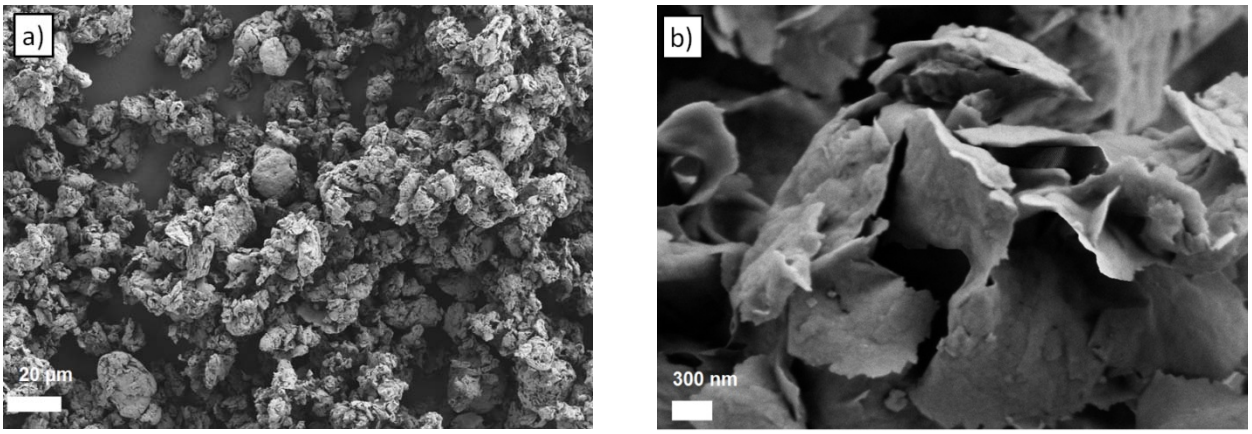

Figure 1**:** SEM picture of clay particle material Cloisite® 15A, Southern Clay Products (today BYK-Chemie). a) 500 times magnification and b) 22000 times magnification

The clay material is present in different shapes. As shown in Figure 1a) there are agglomerates in the micrometer rage which are more or less closely packed. Most clay agglomerates can be described as spherical like structure but there are also units with a significant deviation from the spherical form. Clay particles with diameters in the submicron range are also present. In Figure 1b) in increased view of the clay material reveals the layer structure whereby the layers are adhered to each other and pointing in different directions. The thickness of the layers is a few nanometers and the other two dimensions are in the micrometer range. Therefore the term nanoparticle in relation with clay must be specified i.e. that this material is only in one direction nanoscaled. In order to produce a nanocomposites with the targeted properties these agglomerates must be dispersed with proper extrusion parameters.

For the polymeric matrix a commercial grade of polypropylene (PP) supplied by Dow Chemical was used. Material properties are given in Table 2.

Table 2: Polypropylene matrix material

Tradename	DOW C711-70RNA, Dow Chemical
MFI (230 °C, 2,16 kg)	70 g/min
Density	0,9 g/cm³
Flexural modulus	1250 MPa
Tensile strength	24 MPa

4. Processing of nanocomposite samples

The extrusion of the nanocomposite samples were carried out on a twin screw extrusion line Leistritz 27 HP 52D, Leistritz Extrusionstechnik GmbH, Germany (picture given in electronic supplement). The extrusion line is characterized by a diameter of the screws of 27 mm and a length/diameter ratio of 52 resulting in a processing length of 1404 mm. This size represents an industrial pilot line for small throughputs. A twin screw extruder was chosen for NC production because intercalation and exfoliation of the nanoclays is encouraged by the geometry of rotating double screw [13–16]. Intercalation and exfoliation are important preconditions for complete dispersion of the nanoclays and hence evoke the envisaged material properties of the NC.

The polymer granules and nanoclay powder are fed by a gravimetric dosing (Brabender GmbH, Germany) at the main feeder zone. Depending on the design of the twin screws the material is melted, mixed and forwarded to the extrusion nozzle, where a strand is forwarded to a cooling bath followed by further granulating. The granules were converted to a component part made of the nanocomposite for later use and investigation.

For the spectroscopic in-line measurements two sensors were installed at the extruder die. Two sensors were positioned opposite of each other for transmission measurements. A schematic drawing of the extruder line is given in Figure 2 . For the later validation of the

spectroscopic measurements samples were taken from the polymeric strand after cooling. Particle sizes were measured with scanning electronic microscope (SEM) and compared with results from spectroscopic measurements and their turbidimetric evaluation.

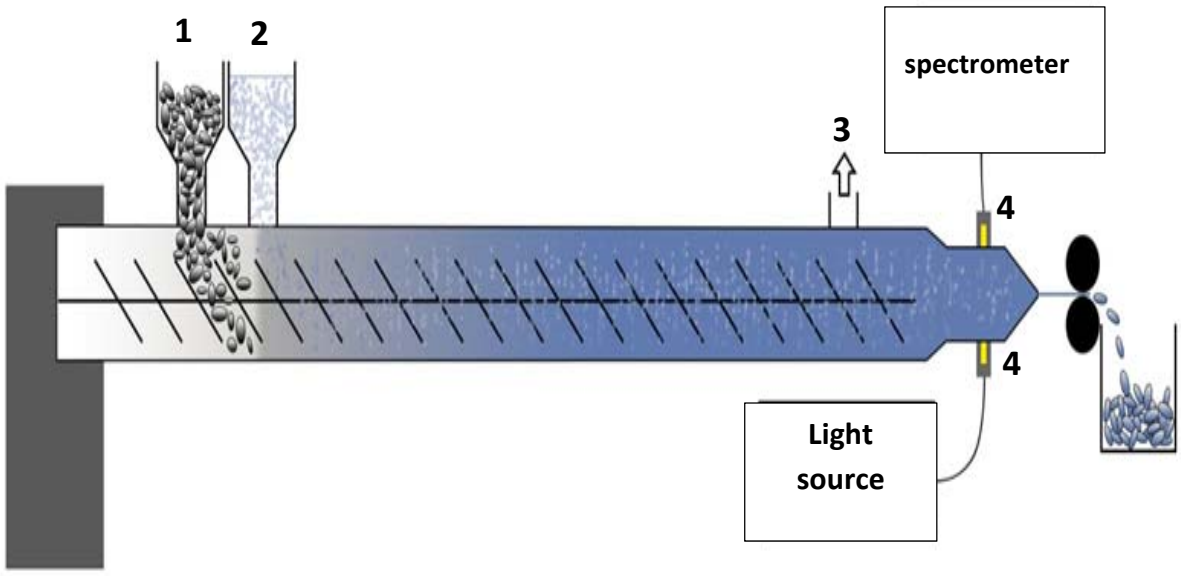

Figure 2: Schematic drawing of extruder line equipped with two optical probes for transmission measurements at the die. There were two dosages one for PP-granulates and one for the Clay particles. There was also a degassing spot to remove air bubbles. (1) Doser for PP granulates; (2) doser for clay pasticles; (3) degassing spot; (4) transmission probes

The spectrometer was a cascaded two unit diode array system MCS600 from Carl Zeiss© (Jena) for the ultraviolette (UV) the visible (Vis) and near infrared (NIR) spectral range from 350 nm to 2100 nm wavelength. The spectral resolution (Rayleigh criterion) was 6 nm in the UV and Vis spectral range and 18 nm in the NIR range. The light source was a 50 [W] halogen lamp. The probes consist of a titan housing with a sapphire window withstanding a temperature of up to 400°C and a pressure of up to 250 bar. These are processing parameters employed in commercial extrusion industry. The distance between the probes was 4 mm.

For the production of the nanocomposite material composition and processing parameter was varied. Nanoclay content in the PP matrix screw speed and throughput was changed in a systematic way and is listed in Table 3. The extrusion temperature was 220°C for all samples.

Table 3: Processing and material variation of the procuced nanocomposites. The parameters are contained in the sample name throughout the rest of the paper.

sample name	throughput [kg/h]	Clay content [wt %]	Screw speed [1/min]
6-0-200	6	0	200
6-1-200	6	1	200
6-1-500	6	1	500
6-1-800	6	1	800
6-3-200	6	3	200
6-3-500	6	3	500
6-3-800	6	3	800
10-1-200	10	1	200
10-1-500	10	1	500
10-1-800	10	1	800
10-3-200	10	3	200
10-3-500	10	3	500
10-3-800	10	3	800

5. Turbidimetric analysis

Turbidimetric analysis can be used for the detection of particle size [4, 11, 17]. The analysis principle is based on the wavelength and particle sizes dependent decrease of light intensity by passing through the sample. The intensity attenuation consists of scattering and absorption and can be mathematical described by the Lambert-Bouguer-relationship, whereas the multiple scattering is neglected [10, 18]:

$$I_T(\lambda_i, l) = I_0(\lambda_i, l) \cdot e^{-N \cdot l \frac{3}{4\pi} \int_{r_{min}}^{r_{max}} C_{Ext}(r,\lambda_i,m) \cdot \frac{p(r)}{r^3} dr} \qquad \text{eq. 1}$$

$\mathrm{I_T}(\lambda_\mathrm{i}, \mathrm{l})$ is the intensity of transmitted light and $\mathrm{I_O}(\lambda_\mathrm{i}, \mathrm{l})$ that of the incident light at a specific wavelength λ_i, N is the volume concentration of the particles, l is optical path length, $\mathrm{C_{Ext}}(\mathrm{r}, \lambda_\mathrm{i}, \mathrm{m})$ is the extinction cross section of the particle with r the particle radius and m the relative refractive index $m = \frac{n}{n_0}$ with n the real refractive of the particle and n_0 that of the surrounding medium. $\mathrm{p(r)}$ is the volumetric distribution of particles.

Using the Mie theory, the extinction cross section $C_{Ext}(r, \lambda_i, m)$ can be calculated recursively [18]. The extinction cross section depends on the polarization and direction of the incoming wave, the particle size, the relative refractive index of particle and of surrounding matrix and the orientation of the particle.

Rearranging ep.1 gives the relationship between experimental and theoretical turbidity leading to eq.2:

$$\tau(\lambda_i) = \frac{1}{l} ln\big(1/T(\lambda_i)\big) = \frac{1}{l} ln\left(\frac{I_0(\lambda_i)}{I(\lambda_i)}\right) = N \cdot \frac{3}{4\pi} \int_{r_{\min}}^{r_{\max}} C_{\mathrm{Ext}}(r, \lambda_i, m) \cdot p(r) \cdot \frac{1}{r^3} dr \qquad \text{eq. 2}$$

To fit the measured turbidity $\frac{1}{l} ln\big(1/T(\lambda)\big)$ to the calculated one the particle radius r in $C_{\mathrm{Ext}}(r, \lambda_i, m)$ and the particle distribution function p(r) must be varied. To vary the particle size distribution p(r) there are several possibilities either by assumption of theoretical distribution curves like e.g. log-normal or the Weibull function [20] or the particle size distribution can be

calculated by solving a linear equation system which we used in the present evaluation. The starting-point of this method is the discretization of equation 2:

$$\tau(\lambda_i) = N \cdot \frac{3}{4\pi} \int_{r_{\min}}^{r_{\max}} C_{\mathrm{Ext}}(r, \lambda_i, m) \cdot p(r) \cdot \frac{1}{r^3} dr = N \cdot \frac{3}{4\pi} \cdot \sum_{j=1}^{m} S_{i,j} \cdot {P_j}^V \qquad \text{eq. 3}$$

where $\mathrm{S_{i,j}}(\lambda_\mathrm{i}, \mathrm{r_j}, \mathrm{m})$ is a discrete $\mathrm{N} \times \mathrm{M}$ extinction cross section matrix with $\mathrm{i} = 1,2, \ldots, \mathrm{N}$ wavelengths and $\mathrm{j} = 1,2, \ldots, \mathrm{M}$ particle radii. ${P_j}^V$ is a discrete particle size distribution.

The problem with these methods is that equation (3) cannot be solved simply by Non Negative Least-Square method (NNLSQ). This problem is known as the ill-posed-problem. The mathematical solution, which allows solving the linear equation system was elaborated by Phillips [21] and Twomey [22]. This is achieved by introducing of a smoothing matrix H and a Lagrange factor $\boldsymbol{\gamma}$. The linear algebraic equation (3) can be described as follows:

$$(S^T \cdot S + \gamma \cdot H)P = S^T \cdot \tau \qquad \text{eq. 4}$$

By minimizing this equation the sought particle size distribution P can be calculated.

$$min_{V \geq 0} \| (S^T \cdot S + \gamma \cdot H)V - S^T \cdot \tau \|_{2-\mathrm{lsq}}^2 \qquad \text{eq.5}$$

More details about this method can be read in [23]. The algorithm was programmed in Matlab© vers.8 (R2016a).

There are several points to be mentioned concerning the correctness of the above equations for describing the turbidity i.e. the light scattering caused by clay particles. The extinction cross section $C_{\mathrm{Ext}}(r, \lambda_i, m)$ is based on Mie calculation for single sphere like particles but clay has a plate like structure with different size in the main distinct directions. The orientations of the clay particles are random therefore one can conclude that there is an average extinction cross section $< C_{\mathrm{Ext}} > = \frac{1}{3} C_{\mathrm{Ext},1} + \frac{1}{3} C_{\mathrm{Ext},2} + \frac{1}{3} C_{\mathrm{Ext},3}$ with $C_{\mathrm{Ext,i}}$ the extinction cross sections in each of

main distinct direction [18]. Hence the modelling and the fitting of the turbidity spectra can yield to a wrong radius distribution of the clay particles. Second there is no interaction between the particles incorporated in the equation which cannot be excluded in the real samples.

Another source of error is the fact that all calculations and parameter like the extinction cross section were done under the assumption of room temperature and normal pressure. But the measurements are performed in an extruder with high pressure and temperature hence optical constants will deviate from literature values. Therefore in section 8 there will a comparison between a SEM picture and the optical method to verify the correctness and usefulness of the proposed method.

6. Results

6.1 SEM pictures of the produced nanocomposites

After processing of the nanocomposites cuts were done from the samples. All SEM pictures and particle evaluation were done with image analyses program “dhs Bilddatenbank”. A SEM picture (Figure 3) was taken from sample “600-1-500” with a magnification of 300. The sample has a homogenous spatial dispersion of the clay in the PP matrix. No bigger agglomerations or clusters are visible. In Figure 4 the same sample is shown with a magnification of 3000. One can see that the clay particles have a plate like shape with thicknesses of the plates in the nanometer range. There are also sphere like particles. The software measured either the length or diameter of the particles and a radius was assigned to every particle on the picture. Enumeration and assignment to classes of radius yields the normalized distribution function. The results of turbidimetric and SEM method could then be compared (Figure 10). The voids are caused by particles which have been ripped off by shearing forces of the extrusion process. The length of the plates is in the range of about 2 µm and lower, respectively. Compared to Figure 1a where the clay starting material is shown no agglomerated structures are visible in Figure 4. That means that the particles have been exfoliated and dispersed through the extrusion process. The particles in Figure 4 are in the size range of 2 µm or lower. They are also aligned in a preferred direction caused by the polymer melt flow during the extrusion. In the electronic supplementary material there is also a picture given of sample “600-1-500” with a magnification of 5000. One can observe that beside the shape like clay particles there are also spherical shaped ones which are in the micrometer and sub-micrometer range.

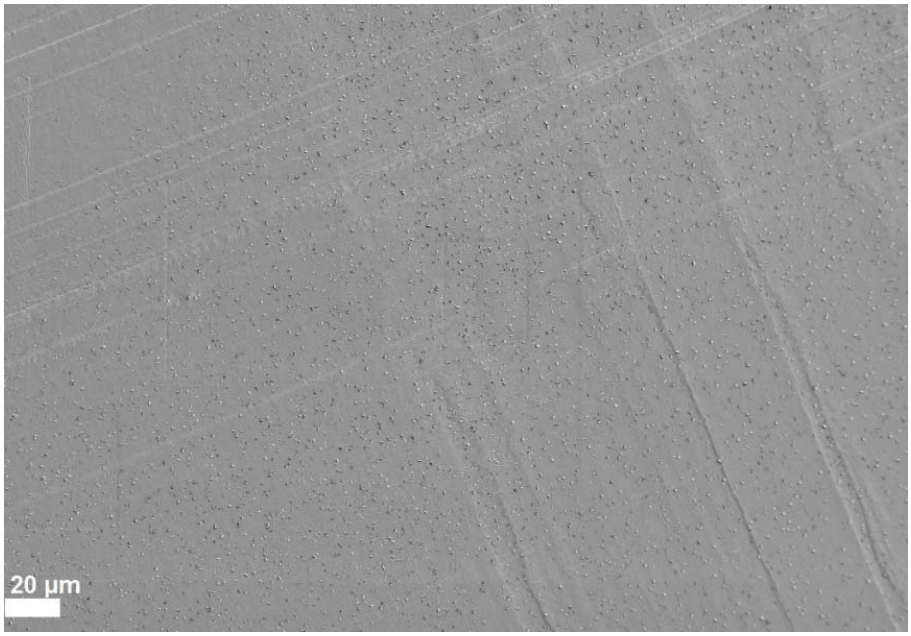

Figure 3: SEM picture of sample „600-1-500“with magnification of 300

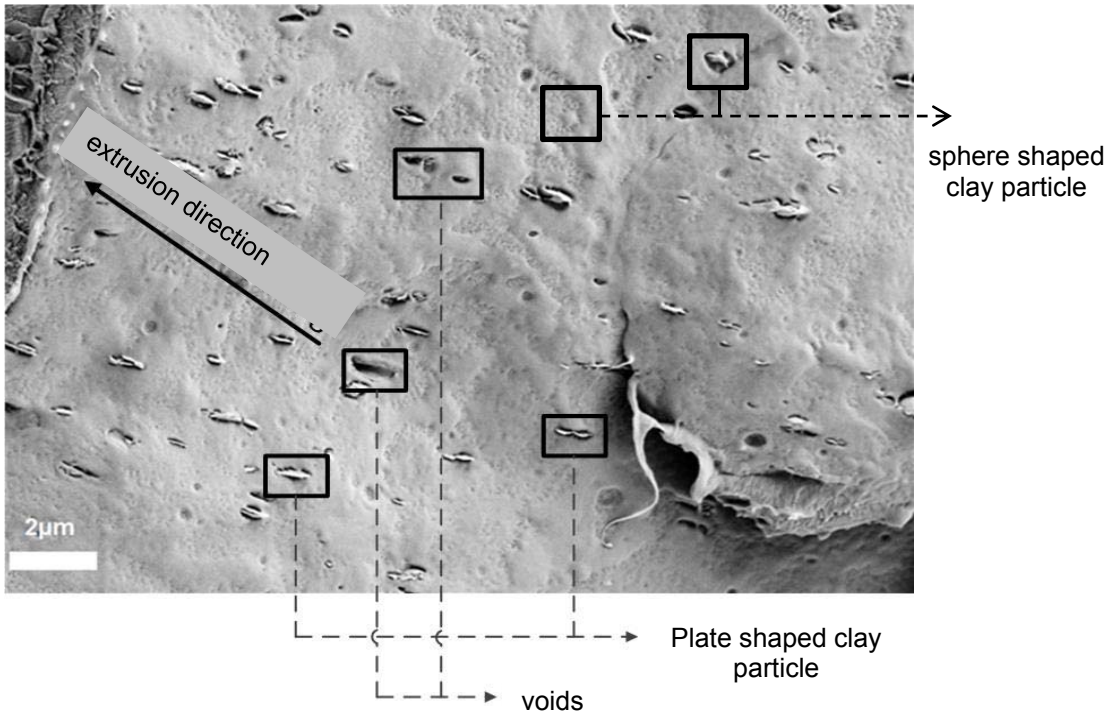

Figure 4: Sample „600-1-500“ with a magnification of 3000

6.2 Transmission spectra of nanocomposites

Spectral in-line measurements were first done with pure PP material as reference and nanoclay was added in subsequent steps. The transmission was calculated according to

$$T = \frac{I_{PP/Clay} - I_D}{I_{PP} - I_D} \qquad \text{eq.6}$$

With T the transmission, $I_{PP/clay}$ the measured intensity spectrum of the sample with concurrent polypropylene / clay mixture and I_D is the dark current measurement.

The results of these in-line measurements are shown Figure 5. The first spectrum 1 is PP against PP and yields a transmission of 1 since no light scattering occurs. After that the extruder was filled with a mixture of PP with 3% (m/m) of nanoclay. Caused by the delay time needed to transport the mixture in the extruder from the dosage unit to the measurement point at the installed probes (see Figure 2) the amount of passing nanoclay is constantly increasing to a maximum of 3% (m/m). This behavior can be seen in Figure 5 where a selection of spectra are shown which are labeled from 1 for pure PP to 4 for maximum amount of 3% (m/m) nanoclay passing the probes.

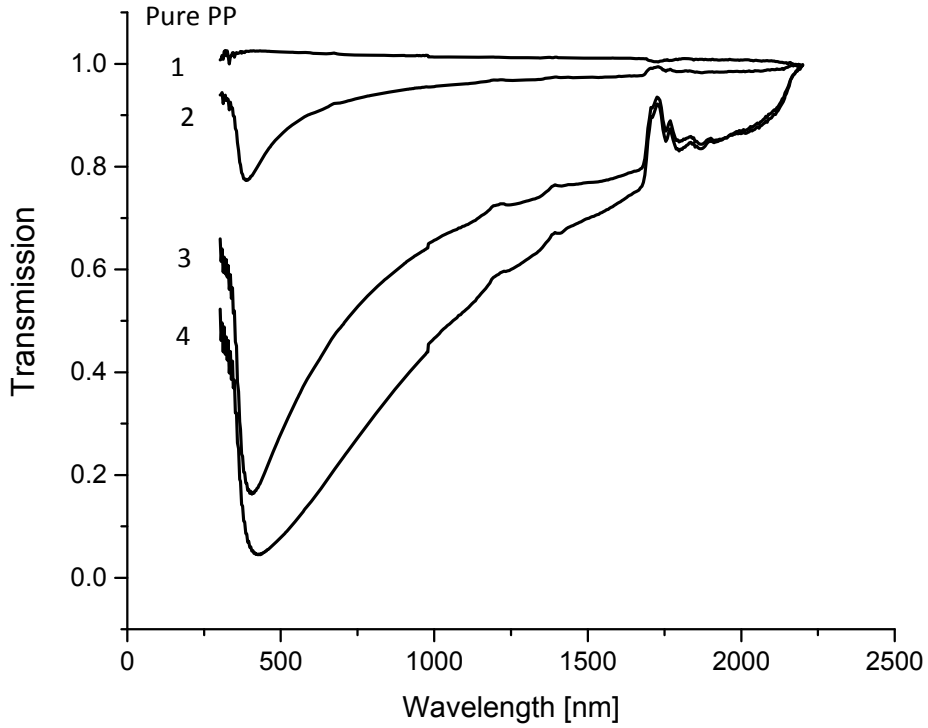

Figure 5: Some spectral in-line transmission measurements of PP / nanoclay mixtures. First spectrum was pure PP. Next PP/ nanoclay mixture with 3% (m/m) nanoclay was added and light scattering is arising causing the typical curvature in the transmission spectra.

The transmission spectra in Figure 5 are dominated by the scattering and absorption effects of the nanoparticles. The curvature between about 500 nm and 1050 nm wavelength is an indication that light scattering is the dominating optical effect in the composite. The absorption band at 380 nm and absorption peak structure at about 1200 nm and 1900 nm can be assigned to spectral characteristics of the nanoclay material (see Figure 6). The absorption peak at 380 nm can be assigned to an electrical charge transfer. The peaks at higher wavelengths are due to absorption of overtone and combination bands which dominate the near infrared spectral range [24].

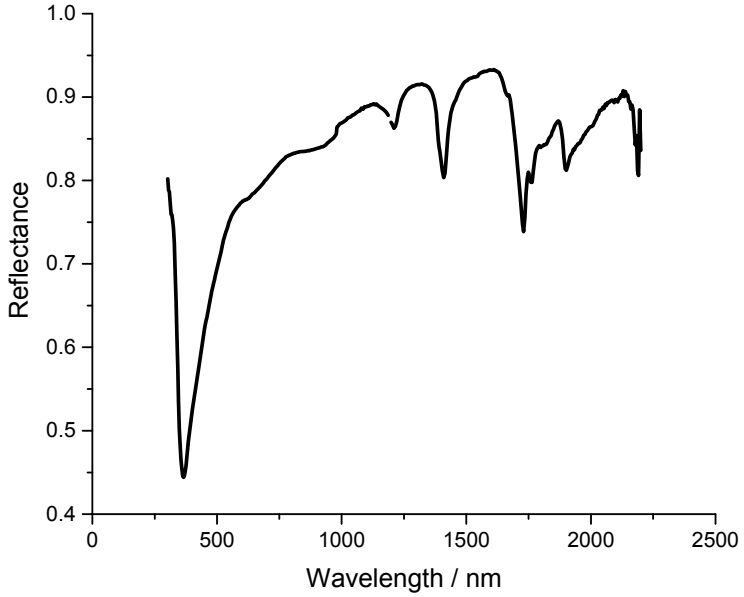

Figure 6: Reflectance spectrum of nanoclay powder in the wavelength range from about 250 nm to 2200 nm used for the preparation of the nanocomposites.

7. Determination of particle size distribution

According to Table **3** samples were prepared with adjusted material (clay concentration) and processing parameters (dosage, screw speed). During the extrusion the transmission spectra were measured when passing the extruder die. After the in-line measurement the spectra were evaluated according to ep.3 in order to yield the particle size distribution density. For the evaluation of the transmission spectra to yield the particle size distribution according to eq.3 the wavelength dependent refractive indices of nanoclay and of PP must be known. For the wavelength dependent refractive index between 400 nm and 1050 nm for the clay particles the values of SiO_2 was taken because it is the main constituent in the clay hence one can assume that optical properties are dominated by it [25]. Values of n_{SiO2} were taken from [26]. Curve is shown in Figure 7.

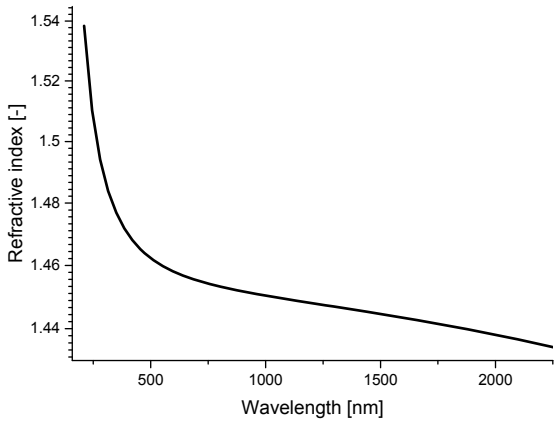

Figure 7: wavelength dependent refractive index of SiO_2.

In the literature there are no standard values of the refractive index for polypropylene (PP) because of the composition of amorphous and crystalline phase which ratio is in the range between 70% and 80% in dependence of production process and application. In most cases a constant value between 1.49 to 1.51 is taken but no wavelength dispersion is given. With constant refractive index the turbidimetric evaluation was unsatisfactory. For the present evaluation the wavelength dependent refractive index was taken from [19] where measurements were done with PP films. Refractive index for PP was 1.5078 for wavelength of

532 nm and 1.5056 for wavelength of 632.8 nm. Only the spectral range from 400 nm to 1050 nm was taken for the determination of particle size. For the description of the absorption peaks in the higher wavelength range of PP and clay the wavelength dependent complex index of refraction $\hat{n} = n + i \cdot \kappa$ with $\cdot\kappa$ the absorption index would be needed for correct description of optical behavior of matter. Because $\cdot\kappa$ is very low for both materials in the used spectral range calculations were done with real refractive index i.e. $\cdot\kappa \approx 0$ and spectral range was limited as described.

The result of samples “6-3-200” and “10-1-500” are shown below in the Figure 8 and in Figure 9 whereby the transmission spectra and the corresponding distribution density for these samples are subsumed. Transmission spectra and corresponding distribution density of samples “6-1-200” and “6-1-500” are given in the electronic supplementary material.

The transmission of sample “6-3-200” shows the typical spectral behavior which is dominated by light scattering of the clay particles. Smaller wavelengths show stronger light scattering than bigger wavelengths hence transmission in the lower wavelength is smaller as can be seen in Figure 8 (left). The increase of the transmission below 500 nm can be ascribed to the peak structure of the clay material in this spectral range (see Figure 6). Turbidity was calculated from transmission data and corresponding distribution density was calculated according to equation 3 (Figure 8 right). As can be seen the distribution density has a bimodal shape with a first peak of particle size of about 2500 nm and a full with at half maximum (FWHM) of about 3500 nm. The second peak of the distribution density function is at about 9500 nm and a width of 3700 nm. In the electronic supplementary material the transmission is shown of sample “6-1-200” and the particle distribution density, respectively. Compared to the transmission spectra of sample “6-3-200” the curvature of sample “6-1-200” is much stronger indicating that light scattering is more intense for samples with lower particle concentration. The same qualitative behavior can be observed in Figure 5 where transmission spectra are shown with increasing clay content from 0% (m/m) to 3% (m/m). The curvature of the transmission curves are correlated with particle content i.e. with higher clay content the transmission spectra are more linear over the wavelength. With higher particle concentration

and particle density the possibility of multi-scattering is strongly increased hence affecting the scattering characteristics which can lead to the observed spectral behavior [27].

The particle distribution density of sample “6-1-200” has also a bimodal behavior but exhibit a gap between the two peaks. The reason for this gap is caused by the numerical iteration procedure in order find a suitable particle distribution function p(r) to fit the measured turbidity (see eq.4). To solve the equation the Langrange factor γ must be chosen properly and a too small γ can introduce small oscillations causing negative values for the distribution density. Unfortunately, the used method does not always guarantee physical reasonable solutions [28]. The mean particle radius in the first peak of the distribution is at about 1500 nm and the FWHM 1400 nm. In the second peak the corresponding values are 10500 nm for the mean particle radius and the FWHM 1000 nm.

The transmission spectra and the corresponding distribution density of sample “6-1-500” is also shown in the supplement. The distribution density shows a monomodal behavior which has a broad peak from about 500 nm to about 1000 nm. The broad peak is an indication that the dispersion process of the clay material did not reach a stable stage.

Sample “10-1-500” shows a bimodal distribution density with a broad band width. The same behavior can be seen of the transmission spectra. The non-completed dispersion process causes this behavior. In the distribution density there is also a gap between the peak for the smaller particles and that of the bigger ones. One can also recognize that within the peaks the distribution is not homogenous. There are crossing points at about 3500 nm and at 10000 nm.

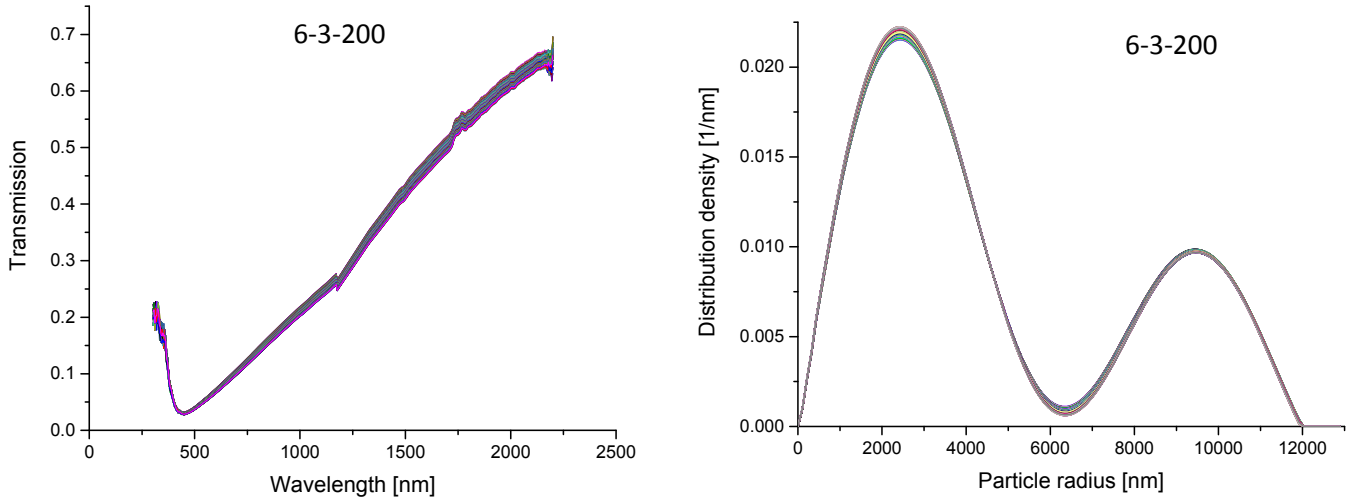

Figure 8: Measured transmission spectra of sample 6-3-200 (left) and deduced particle size distribution density (right).

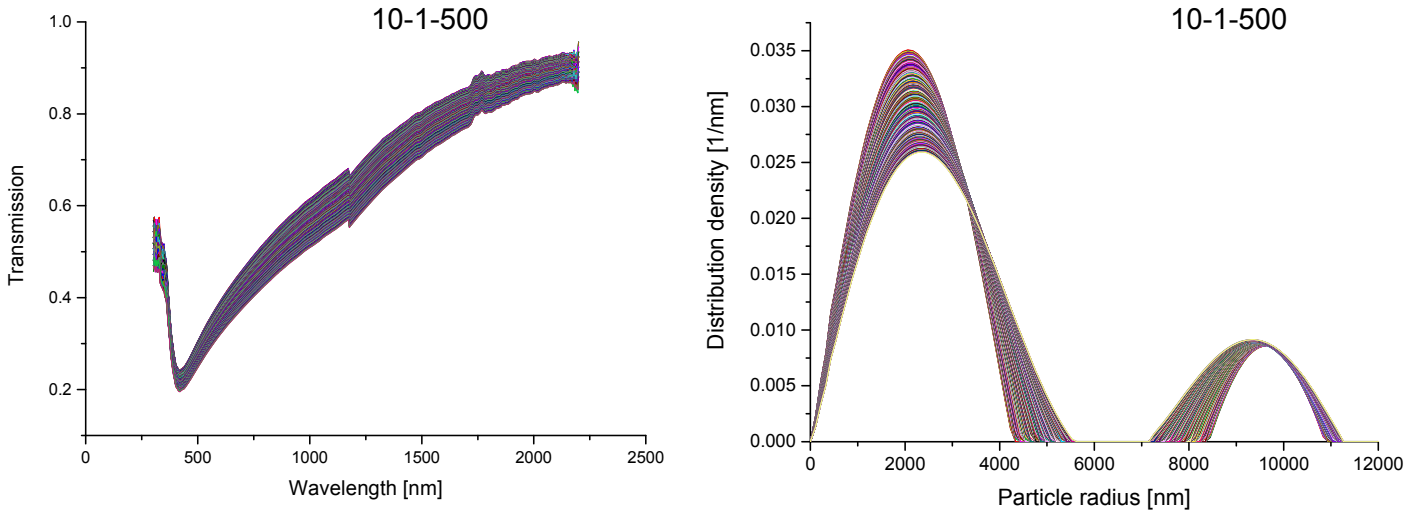

Figure 9 Measured transmission spectra of sample 10-1-500 (left) and deduced particle size distribution density (right).

8. Verification of the method

To verify the correctness of the turbidimetric method, the size distributions in the nanocomposites were also determined by scanning electron microscopy (SEM). Therefore the sample “6-1-500” was chosen because the sample showed a monomodal distribution and both analytic methods have been directly compared with each other. The transmission spectra and deduced particle density are given in the electronic supplementary. In the present case a Zeiss SUPRA 55VP was used for the SEM measurement. The result is shown in Figure 10. Maximum value of the distribution functions were normalized to one. It is obvious that the width of both distribution functions is in the same range and the median particle radius is also the same range. As mentioned above small errors like noisy measurement and the free parameter γ is an undetermined Langrange multiplier which produces “tensions” in the curve fit. Choosing a too small γ can lead to false oscillations into the solution hence resulting into negative solutions. But also the SEM measurement shows that the particle distribution approaches low numbers and the overall shape of the distribution functions from both analytical methods reveal the same qualitative results.

There are several factors which can lead to strong deviations between optical measurement and the fitting. The extinction cross section $C_{Ext}(r, \lambda_i, m)$ which is the kernel in the integral equation 2 is assumed for single scattering for every particle. For nanocomposite samples with high nanoclay content it cannot be excluded that multiple scattering occurs falsifying the fitting. Furthermore the extinction cross section is based on Mie theory assuming sphere like scatterers but the nanoclay possesses a plate like structure. The measurements were done at relatively high temperatures but optical parameters like refractive index for room temperature were taken. Nevertheless the turbidimetric measurement and the evaluation with the linear inversion according to equation 3 deliver comparable results to SEM particle determination. Hence the used method delivers reasonable results for the particle characterization in the nanocomposite during extrusion and can be used as a rugged process measurement system.

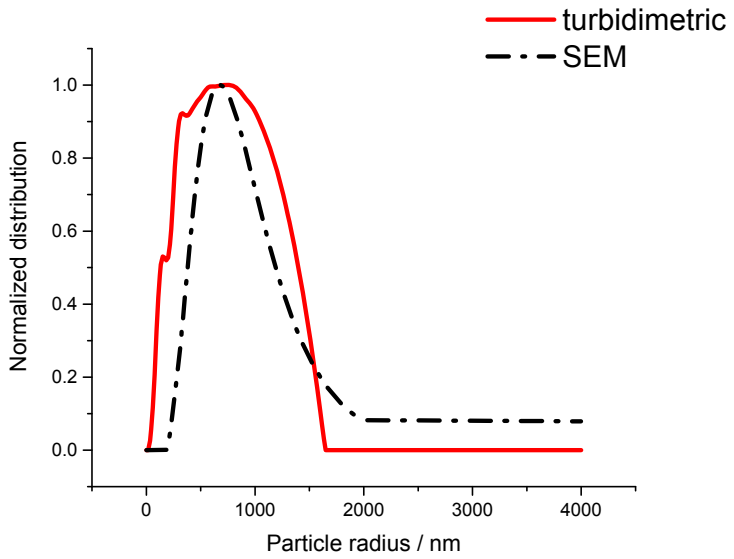

Figure 10: Comparison of particle density distribution received with turbidimetric method and SEM. Measurements done with sample “6-1-500”.

9. Dispersion dynamic of particles

Comparing the distribution densities of sample “10-1-500” (Figure 9) and that of sample “6-1-200” (Figure 8) one can see that there is an obvious difference in the dynamic behavior of this quantity. The band width of the distribution density of sample “10-1-500” is bigger compared to that of sample “6-3-200”. The broader band width indicates that the extrusion process and hence dispersion of the clay particles has a higher dynamic and exhibits no stable process. The evolving dispersion density of sample “10-1-500” is shown in Figure 11 and that of sample “6-3-200” in Figure 12. For both samples the curves of the distribution densities are shown in the beginning and in the mean (only sample “10-1-500”) and at the end of the extrusion process. In one can see that with increasing extrusion duration the height of the peak spanning the smaller particles in sample “10-1-500” from 0 nm to about 4000 nm is decreasing and at the same time the width is increasing to bigger particle radii. Conversely the height of peak encompassing the bigger particles in the sample from about 8500 nm to 11000 nm remains

the same but the width is also increasing but to smaller particle radii. That means that the dispersion process has not come to a stable stage during the extrusion process. There are still deagglomeration mechanisms from bigger particles to smaller ones and agglomeration processes from smaller to bigger ones.

The time dependent distribution density function of sample “6-3-200” shows a much weaker variation. Between the starting and the end curve there is only a slight difference. But a more detailed inspection of the curves show that there is a convers effect concerning the increase and decrease of the peaks representing smaller and bigger particles. The peak from 0 nm to about 5000 nm is increasing a little bit whereby the width of the peak between about 8000 nm to 12000 nm is decreasing. Bigger particles are grinned to smaller ones. But compared to sample “10-1-500” the dynamic is much weaker and the extrusion process is much more stable.

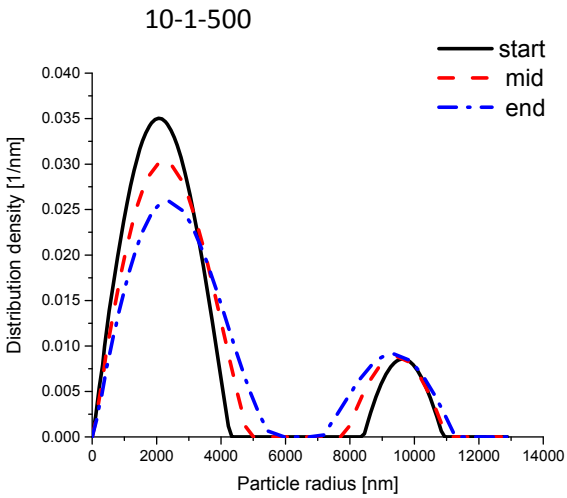

Figure 11: Display of start, mean and end distribution densities of sample „10-1-500“

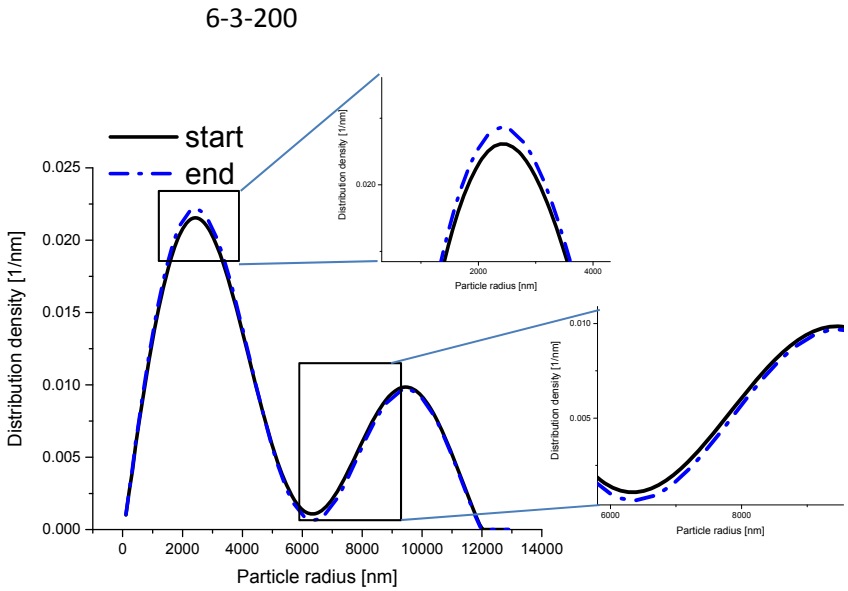

Figure 12: Display of start and end distribution densities of sample „6-3-200“. Details of the peak of curves are shown in the enlarged views.

10. Processing Application

Beside the investigation of the dispersion behavior of nanoclay in a polymer matrix in dependence of specific processing and material properties the crucial question is the suitability for industrial in-line monitoring of this method. First the mean particle diameter was calculated as the average of all measurements regardless whether there was a bimodal or monomodal distribution density. This simplification and reduction of the information of the particle radii can be accepted because the mean particle radius allows the monitoring of the dispersion process and consequently the condition of the nanocomposite. Based on a comprehensive characterization of the whole process with a design of experiment the received mean particle radius and its time behavior can serve as a key parameter to conclude to other properties like e.g. whether there is a bimodal distribution or not.

Figure 13 shows the deduced particle size distribution of nano-clay particles with different parameters settings over the whole extrusion process. It can be clearly recognized that the parameters settings have a significant influence on the distribution of nano-clay particles in the polymer matrix. The concentration is a major influence on dispersion of clay particle in the polymer. In samples with 1 % of clay particle content the variation of experimental parameters (screw speed and through put) led to a strong variation in particle size. By contrast, the samples with 3 % of clay particle show only modest differences. This illustrates the relationship between the processing parameters and middle particle radius. Sample “10-1-500” shows a broad particle dispersion over time indicating the high dynamic of this sample.

Beside a pure dispersion monitoring there is also the possibility to control and adjust material properties like e.g. viscosity or rheological values like E-module or tensile strength. Regression could be done via multivariate methods like partial least spare regression [29]. After implementing prediction models which correlate dispersion state and the regarding material values product properties could be controlled directly. Thus extrusion processing controlled by

“feed forward concept” would be possible [30]. Thus faster and waste avoiding production can be implemented and product properties can be surveyed in-line.

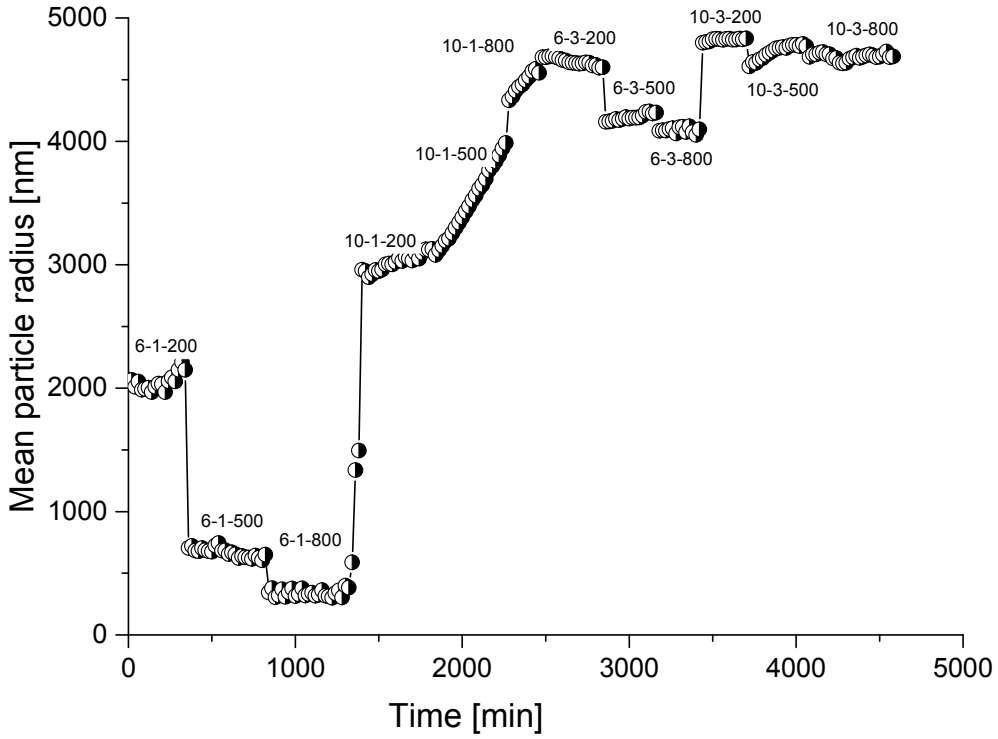

Figure 13: Mean particle radius over extrusion time. The extrusion processing parameters and the dosage are indicated at every sample

11. Conclusions

The main aim of the work was to investigate the capabilities of the optical spectroscopy sensing system for the inline characterization of clay nanocomposites concerning nanoparticle size distribution during extrusion. Test measurements were performed on a laboratory extruder whereby transmission spectra were recorded of samples where processing and material parameters were varied systematically. The turbidimetric measurement method together with numerical version of the Fredholm integral equation of the first kind was successful applied to reveal the distribution density p(r). Because not a fixed distribution function like log-normal or Weibull is specified but the distribution function p(r) is determined by fitting the measured transmission to the theoretical description of the light scattering by Mie theory. Hence particle dispersion and dynamic during extrusion is observable.

This system allows on the one hand quality monitoring during processing but on the other hand enables quick and cost efficient material development. The influence of process parameters on the distribution of the nanomaterial in the polymer matrix can be monitored in real time.

The main limitations are the degree of transparency needed and therefore the maximum concentration of the nanoparticles in the polymer matrix as well as week scattering materials. This can be overcome by using a smaller distance between the sensors (e.g. by using a specific nozzle design) or by enlarging the wavelength range by using UV spectrometers, respectively.

As leading to a highly cost efficient process but also to deep understanding of material structure/property relationship, this will contribute to the introduction of this material class to new applications.

To investigate the dispersion process of clay particles extrusion time and parameters must be varied in a more comprehensive way like in a design of experiment. From the presented measurements and their dynamic it can be concluded that there is a permanent process of agglomeration and de-agglomeration. This dynamic process must be properly controlled to achieve a stable and reproducible production process and product properties. The presented method and process therefore is also an important contribution to quality insurance.

Compliance with Ethical Standards

Conflict of interest
The authors declare that they have no conflict of interest

12. References

1. Jordan J, Jacob KI, Tannenbaum R, Sharaf MA, Jasiuk I (2005) Experimental trends in polymer nanocomposites—a review. Materials Science and Engineering: A 393(1-2):1–11
2. Paul DR, Robeson LM (2008) Polymer nanotechnology. Nanocomposites. Polymer 49(15):3187–3204
3. Schönfeld S (2003) Nanocomposites. Special:28–33
4. Apfel U (1994) A Turbidity Study of Particles Interaction in Latex Suspensions. Colloid Polym Sci
5. Rohe T, Becker W, Krey A, Nägele H, Kölle S, Eisenreich N (1998) T.Rohe in-line monitoring of polymer extrusion processes by NIR spectroscopy. Near Infrared Spectrosc.(6):325–332
6. Rohe T, Kölle S (2000) Inline nahinfrarotspectroskopie bei der kunststoffextrusion. GIT Labor-Fachzeitschrift
7. Becker W, Eisenrich N (2005) Measurement of the Irganox content in polypropylene polymers during extrusion. J. Near Infrared Spectrosc. 13(1):147
8. Rohe T, Kölle S, Stern C, Eisenreich N, Eyerer P (2001) Inline near infrared(NIR) spectroscopy for application in polymer extrusion processes. Recent Res. Devel. Pure & Applied Anal. Chem.(3)
9. Furukawa T (2002) On-line monitoring of melt extrusion transesterification of ethylene vinylacetate copolymers by near infrared spectroscopy and chemometrics. Journal of Near Infrared Spectroscopy:195–202
10. Kerker M, Loebl EM (1969) The Scattering of Light and Other Electromagnetic Radiation. Physical Chemistry: A Series of Monographs. Elsevier Science, Burlington
11. Berdahl P, near infrared turbidity of ß-FeOOH particle suspensions (2000), Appl. Spectroscopy 54(2).,
12. Apfel U (1995) Precise Analysis of the Tubidity Spectra of a Concentrated Latex. Langmuir 11
13. Kohlgrüber K (2012) Co-Rotating Twin-Screw Extruder. Carl Hanser Verlag GmbH & Company KG
14. Nguyen QT, Baird DG (2007) An improved technique for exfoliating and dispersing nanoclay particles into polymer matrices using supercritical carbon dioxide. Polymer 48(23):6923–6933
15. Wang Y, Chen F-B, Wu K-C (2004) Twin-screw extrusion compounding of polypropylene/organoclay nanocomposites modified by maleated polypropylenes. J. Appl. Polym. Sci. 93(1):100–112
16. Peltola P, Välipakka E, Vuorinen J, Syrjälä S, Hanhi K (2006) Effect of rotational speed of twin screw extruder on the microstructure and rheological and mechanical properties of nanoclay-reinforced polypropylene nanocomposites. Polym. Eng. Sci. 46(8):995–1000
17. Kerker M (1969) The scattering of light and other electromagnetic radiation. Physical chemistry, vol. 16. Acad. Press, New York
18. Bohren CF, Huffman DR (2007) Absorption and scattering of light by small particles. Wiley-VCH, Weinheim
19. Yovcheva T (2008) Refrextive index of corona-trated polypropylene films. Jounanl of Optics A: Pure and Applied Optics(10)
20. Guschin V, Becker W, Eisenreich N, Bendfeld A (2012) Determination of the Nanoparticle Size Distribution in Media by Turbidimetric Measurements. Chem. Eng. Technol. 35(2):317–322
21. Phillips DL (1962) A Technique for the Numerical Solution of Certain Integral Equations of the First Kind. J. ACM 9(1):84–97

22. Twomey S (1975) Comparison of constrained linear inversion and an iterative nonlinear algorithm applied to the indirect estimation of particle size distributions. Journal of Computational Physics 18(2):188–200
23. Guschin V (2016) Kombination von turbidimetrsichen Methodenmit Verfahren der multivariaten Datenanalyse zur Prozesscharakterisierung von Nanokompositen. doctor thesis Fakultät für Maschinenbau Karlsruher Institut für Technologie (KIT)
24. Workman J, Weyer L (2012) Practical guide and spectral atlas for interpretive near-infrared spectroscopy, 2nd ed. CRC Press, Boca Raton, FL
25. Alig I, Steinhoff B, Lellinger D (2010) Monitoring of polymer melt processing. Meas. Sci. Technol. 21(6):62001
26. Polyanskiy MN (2016) Refractive index database, http://refractiveindex.info
27. Kortüm G (1969) Reflexionsspektroskopie. Grundlagen, Methodik, Anwendungen. Springer, Berlin, Heidelberg
28. Steele HM, Turco RP (1997) Retrieval of aerosol size distributions from satellite extinction spectra using constrained linear inversion. J. Geophys. Res. 102(D14):16737–16747
29. Kessler W (2006) Multivariate Datenanalyse für die Pharma-, Bio- und Prozessanalytik. Ein Lehrbuch. Wiley-VCH, Weinheim
30. Kessler RW (ed) (2006) Prozessanalytik. Strategien und Fallbeispiele aus der industriellen Praxis. Wiley-VCH, Weinheim